

Combined Atom-Transfer Radical Polymerization and Ring-Opening Polymerization to Design Polymer–Polypeptide Copolymer Conjugates Toward Self-Aggregated Hybrid Micro/Nanospheres for Dye Encapsulation

Anupam Saha, Tapas K. Paira, Mrinmoy Biswas, Somdeb Jana, Sanjib Banerjee, Tarun K. Mandal

Polymer Science Unit, Indian Association for the Cultivation of Science, Jadavpur, Kolkata 700 032, India
Correspondence to: T. K. Mandal (E-mail: psutkm@iacs.res.in)

Received 8 April 2015; accepted 28 May 2015; published online 17 June 2015

DOI: 10.1002/pola.27713

KEYWORDS: aggregation; ATRP; bioconjugate; biopolymers; diblock copolymers; micro/nanostructures; nanoparticles; polymer-polypeptide; ROP

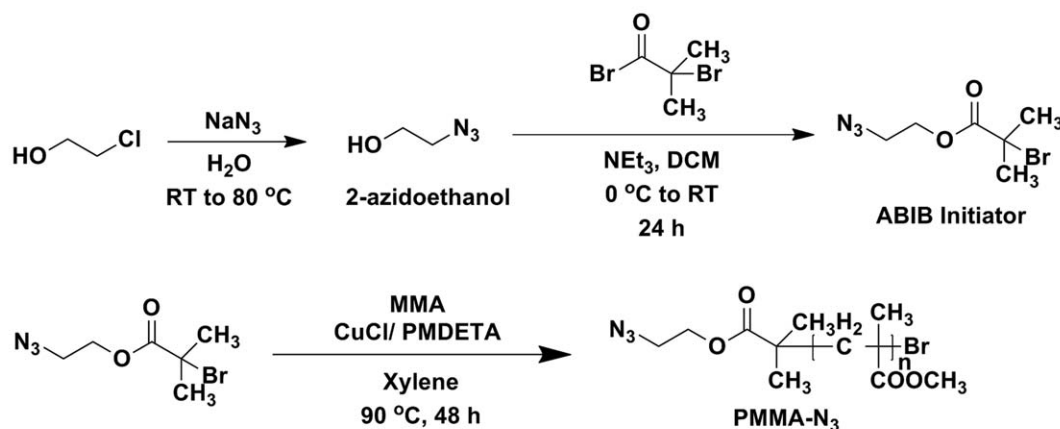
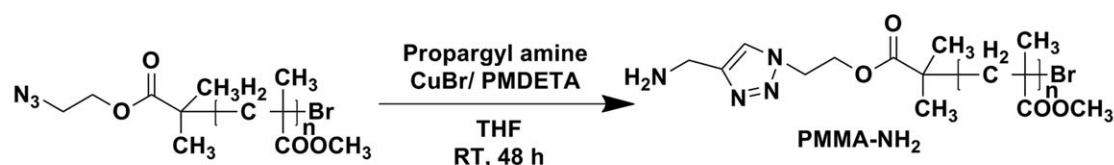
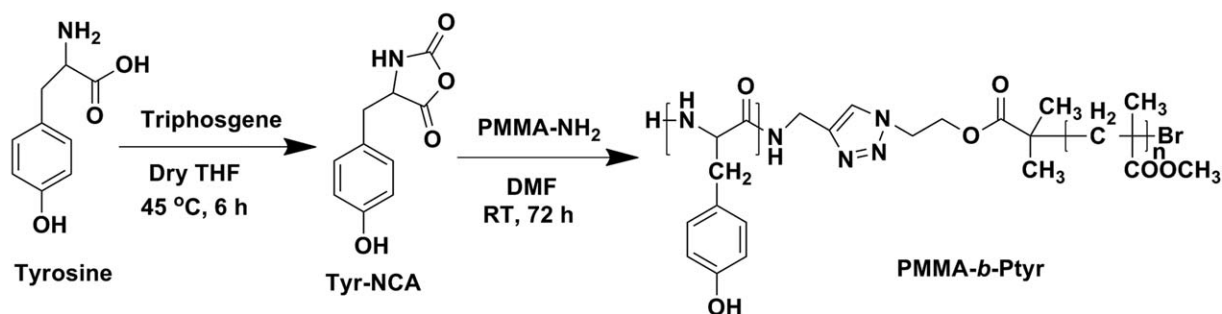
INTRODUCTION In present decades, interest in combining polypeptides/peptides of precise chemical structure and functionality with stable and processable synthetic polymers has been growing rapidly.^{1–3} The presence of the peptide segment can introduce biocompatibility, bioactivity, and self-assembly property in such conjugate materials.^{4–6} Although the introduction of the synthetic polymeric component controls the overall physical and chemical properties of the conjugate materials.⁷ Such conjugate materials have potential wide-ranging biomedical,⁸ tissue engineering,⁹ biomaterial, and drug-delivery applications.¹⁰ Furthermore, peptide–polymer conjugates may enable them to self-assemble into functional well-defined micro/nanostructured biomolecular materials with great implications in both biological^{11,12} and nonbiological applications.^{13–15}

There have been tremendous developments in recent years in the synthetic tool box available to polymer chemists with the introduction of controlled radical polymerization (CRP), which allows superior control over molecular weights, molecular weight distribution, and microstructure.^{16–18} Consequently, there has been easy access to block copolymers that has huge importance from the standpoint of creating nanostructured polymeric materials.^{19,20} In particular, several groups including our group put emphasis on the use of CRP techniques such as atom-transfer radical polymerization (ATRP) to prepare polypeptide/peptide-based block copolymer conjugates.^{16,21,22} It is also known that ring-opening polymerization (ROP) of α -amino acid *N*-carboxyanhydride (NCA) initiated by nucleophiles or bases is the most common

technique to synthesize different polypeptides.^{23,24} In general, polymer–peptide/polypeptide conjugates are synthesized by “grafting from” technique instead of “grafting to” involving the following two protocols: (1) it is the preparation of the sequence-defined peptide segment by solid/solution-phase route followed by its transformation into macroinitiators for ATRP of various vinyl monomers to synthesize desired peptide–polymer conjugates,^{25–27} (2) it is the synthesis of amino acid NCAs followed by its ROP using amino-terminated synthetic polymers to polypeptide–polymer block copolymer conjugates.²⁸ Thus, several different techniques have been employed to synthesize polypeptide/peptide–polymer conjugates of various polymers and peptides and investigated their self-aggregation behavior in different solvents.^{29–31} Nagai et al.³¹ used di-*tert*-butyltricarboxylate to prepare NCAs and synthesized poly(α -amino acid)s. Lu et al.³² synthesized polytyrosine by ROP using propargyl amine as initiator and blended the polypeptide with poly(4-vinylpyridine) in dimethylformamide (DMF) and MeOH solutions. Klok et al.²⁹ synthesized (styrene)₁₀-*b*-poly(γ -benzyl-L-glutamate) conjugates via ROP of γ -benzyl-L-glutamate NCA using primary amine-terminated oligo(styrene) as the initiator and studied the self-assembly of diblock copolymers. Huang and Chang³⁰ reported the synthesis of stimuli-responsive poly(*N*-isopropylacrylamide)-*b*-polylysine copolymer and investigated their self-aggregation behavior. It has been reported by many groups that polymer-*block*-peptide/polypeptides conjugate can easily undergo self-aggregation into micelles,^{33,34} vesicles,³⁵ and different microstructures³⁶ in both aqueous and nonaqueous medium. In

Additional Supporting Information may be found in the online version of this article.

© 2015 Wiley Periodicals, Inc.

Step I: Synthesis of 2-azidoethyl 2-bromoisobutyrate (ABIB) initiator and PMMA-N₃**Step II: Synthesis of PMMA-NH₂****Step III: Preparation of Tyr-NCA and PMMA-*b*-Ptyr conjugate**SCHEME 1 Synthesis pathways for PMMA-*b*-Ptyr block copolymer conjugate.

this context, previously, we reported the synthesis of conjugates comprising sequence-defined short peptide and polymer using ATRP/ROP techniques and their self-aggregation into micro/nanospheres in different polar organic solvents.^{26,37} We thought that it would be interesting to synthesize polymer–polypeptide conjugates and to study their self-aggregation behavior in different solvents.

Herein, we report the synthesis of poly(methyl methacrylate)-*b*-polytyrosine (PMMA-*b*-Ptyr) copolymer conjugate from a designed orthogonal dual initiator via the combination of ATRP of methyl methacrylate (MMA), “click” chemistry and ROP of tyrosine–NCA. We further investigate the self-aggregation behavior of the as-synthesized PMMA-*b*-Ptyr bioconjugate in DMF, which exhibits the formation of micron/nanometer-sized spherical aggregated structures as examined through field emission scanning electron microscopy (FESEM) and dynamic light scattering (DLS).

The effect of copolymer compositions on the self-aggregation behavior is also investigated. PMMA-*b*-Ptyr conjugates of shorter PMMA blocks are soluble in alkaline water of pH 12.5, which further permits the study of its aggregation in water. The formation of composite micellar structures is justified by dye encapsulation study of rhodamine-6G (R6G), a model dye, into the aggregated PMMA-*b*-Ptyr microspheres via fluorescence microscopy and time-correlated single-photon counting (TCSPC) technique.

RESULTS AND DISCUSSION**Synthesis of PMMA-*b*-Ptyr Conjugate**

Our approach to synthesize the copolymer consisting of PMMA and Ptyr blocks involved the following steps: (1) synthesis of azide end-functional orthogonal ATRP initiator followed by the polymerization of MMA to synthesize azide-terminated PMMA (PMMA-N₃) (Step I of Scheme 1), (2)

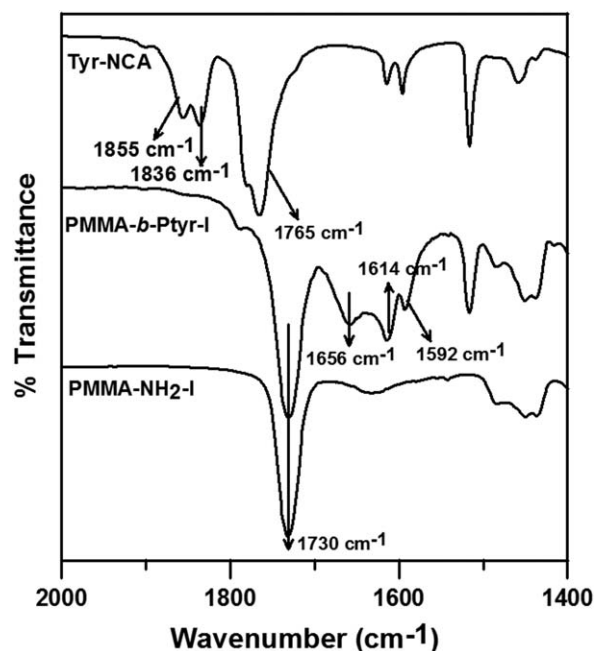


FIGURE 1 FTIR spectra of PMMA-NH₂-I, PMMA-*b*-Ptyr-I conjugate, and tyrosine-NCA.

conversion of azide-terminated PMMA to amine-end functional PMMA (PMMA-NH₂) via the Huisgen's 1,3-dipolar cycloaddition (Step II of Scheme 1), (3) ROP of tyrosine-NCA from the as-synthesized macroinitiator PMMA-NH₂ to obtain PMMA-*b*-Ptyr (Step III of Scheme 1) conjugate. First, we prepared 2-azidoethanol by the reaction of 2-chloroethanol with sodium azide followed by its conversion into 2-azidoethyl 2-bromoisobutyrate (ABIB) via coupling reaction with α -bromoisobutyryl bromide (Step I of Scheme 1). The obtained 2-azidoethanol and ABIB were characterized by FTIR and ¹H-NMR (Supporting Information Figs. S1 and S2). ATRP of MMA was then performed using ABIB initiator to synthesize PMMA-N₃. The FTIR spectrum of PMMA-N₃ showed characteristic bands at 2104 and 1730 cm⁻¹ corresponding to the stretching frequencies of azide and ester groups, respectively (Supporting Information Fig. S1). We finally synthesized three samples namely, PMMA-N₃-I, PMMA-N₃-II, and PMMA-N₃-III of different molecular weights simply by varying the monomer-to-initiator ([M]₀/[I]₀) ratio as listed in Supporting Information Table S1. Our intention was to check the relative reactivities of these macroinitiators (after transforming into PMMA-NH₂)

toward the ROP of tyrosine-NCA and to prepare the conjugates of varying lengths of PMMA blocks. The average molecular weights of the obtained PMMA-N₃-I, PMMA-N₃-II, and PMMA-N₃-III were found to be 7.0, 4.2, and 3.0 kDa with low polydispersity indices (PDIs) of 1.35, 1.22, and 1.25, respectively (chromatograms; Supporting Information Table S1 and Figure S3), indicating the controlled nature of the polymerization. It should be noted that there was a little deviation from the theoretically calculated molecular weights and the experimentally observed molecular weights (Supporting Information Table S1).

Furthermore, in the second step, PMMA-N₃s were coupled with propargyl amine via "click" reaction to produce PMMA-NH₂ (Scheme 1), an active macroinitiator for growing polytyrosine through ROP of tyrosine-NCA. As shown in Figure 1, there was a complete disappearance of the band at 2104 cm⁻¹ for azide group in the FTIR spectrum of a representative sample (PMMA-NH₂-I), indicating complete transformation of PMMA-N₃ to PMMA-NH₂.

To afford the synthesis of PMMA-*b*-Ptyr conjugates, in the third step, we first prepared tyrosine-NCA from ring closing of tyrosine using triphosgene as shown in Step III of Scheme 1. FTIR (Fig. 1) and ESI-mass spectrum (Supporting Information Fig. S4) established the formation of tyrosine-NCA. The ROP of tyrosine-NCA was then performed with PMMA-NH₂s of varying block lengths as macroinitiators to obtain PMMA-*b*-Ptyr conjugates of different molecular weights. FTIR spectra (Fig. 1) showed that the band of amide group of NCA ring at 1765 cm⁻¹ was totally shifted to 1656 cm⁻¹ (amide I for polypeptide segment), whereas the band of -COOCH₃ group of PMMA at 1730 cm⁻¹ remained unaltered in PMMA-*b*-Ptyr-I conjugate, which indicated the formation of Ptyr block at the end of PMMA block.

¹H-NMR spectrum (Supporting Information Fig. S5) of PMMA-*b*-Ptyr-I revealed signals at δ = 3.545 ppm for methyl ester protons of PMMA, 6.62–6.68 and 7.02–7.07 ppm for aromatic protons of tyrosine ring, 7.935 ppm for tyrosinate proton, and 9.26–9.34 ppm for amide protons of Ptyr along with all expected signals which confirmed the attachment of Ptyr block with PMMA block. We also observed similar signals for other two conjugates (PMMA-*b*-Ptyr-II and PMMA-*b*-Ptyr-III) (Supporting Information Fig. S6). Table 1 lists the molecular masses of all three conjugates calculated from proton integration value of tyrosine and MMA units

TABLE 1 ROP Conditions of Tyrosine-NCA Using PMMA-NH₂ Macroinitiator for PMMA-*b*-Ptyr Conjugates and Their Molecular Weight Analysis Data^a

Sample Name	Macroinitiator	[M] ₀ /[I] ₀	Conv. (%)	M _{n, theo.} (kDa) ^b	M _{n, NMR} (kDa)	M _{n, GPC} (kDa)	PDI
PMMA- <i>b</i> -Ptyr -I	PMMA-NH ₂ -I	45	50	11.05	12.2	11.8	1.30
PMMA- <i>b</i> -Ptyr -II	PMMA-NH ₂ -II	60	62	10.95	15.9	–	–
PMMA- <i>b</i> -Ptyr -III	PMMA-NH ₂ -III	60	50	8.45	12.9	–	–

^a Conditions: [I]₀ = [PMMA-NH₂-I]₀ = 1 wt % (w/v); solvent = DMF; temperature = room temperature; reaction time = 72 h.

^b The calculation of M_{n, NMR} is given in page S6 of Supporting Information material.

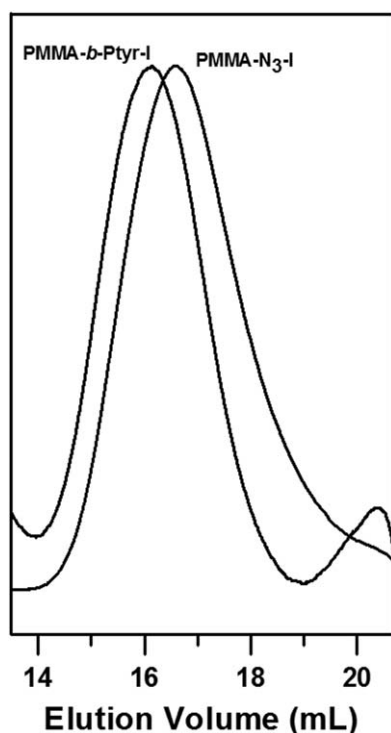


FIGURE 2 GPC traces of PMMA-N₃-I and PMMA-*b*-Ptyr-I conjugate.

from ¹H-NMR spectra using the equation given in the Supporting Information material.³⁸ For the calculation of M_n , we determined the number of MMA units present in all three PMMA-N₃s from gel permeation chromatography (GPC) data instead of ¹H-NMR data, which is the same as number of MMA units in the macroinitiator (Supporting Information material). Because of the reason that we were unable to find any distinguished signal of PMMA macroinitiator in all the conjugates, the obtained molecular weight of the conjugate from ¹H-NMR data is actually average molecular weight which is correlated with the theoretically calculated value (Table 1).

The GPC trace of PMMA-*b*-Ptyr-I was unimodal and symmetrical, the analysis of which gave a M_n of 11.8 kDa and PDI of 1.30 (Fig. 2). Figure 2 clearly also reveals a shift of GPC trace of PMMA-*b*-Ptyr-I toward higher molar mass region which accounts for 4.8 kDa, compared to that of PMMA-N₃-I after ROP of tyrosine-NCA with PMMA-NH₂-I macroinitiator. This further indicated the formation of PMMA-*b*-Ptyr block copolymer. For PMMA-*b*-Ptyr-I sample, there was a quite good agreement between the M_n measured from GPC and calculated from the aforementioned NMR (Table 1 and Table S2). However, we were unable to calculate M_n s of PMMA-*b*-Ptyr-II and PMMA-*b*-Ptyr-III, where the Ptyr block lengths are comparatively higher than that in PMMA-*b*-Ptyr-I. This difficulty may arise owing to the increase of interaction among Ptyr block of PMMA-*b*-Ptyr conjugate.³² Therefore, instead of M_n , GPC, we provided their molecular weights as the measurement from ¹H-NMR analysis (Table 1).

Self-Aggregation Behavior of PMMA-*b*-Ptyr Conjugates

It is well known that polymer-peptide/polypeptide bioconjugates have very high tendency toward self-aggregation in solution.^{39,40} Thus, we explored the self-aggregation behavior of the as-synthesized PMMA-*b*-Ptyr conjugate in DMF. The FESEM images (Fig. 3) of PMMA-*b*-Ptyr-1 revealed the formation of micro/nanospheres in DMF. To check the morphology evolution with time, we also examined DMF solution of PMMA-*b*-Ptyr-1 conjugate, drop-casted at different time intervals of 30 min, 4 h, and 24 h, respectively, via FESEM. We observed the formation of self-aggregated micro/nanospheres with an average diameter of 121, 345, and 750 nm for the sample drop-casted after at 30 min, 4 h, and 24 h, respectively (Fig. 3), indicating the increment of size with time. The histogram of particle size distributions at different time intervals is also shown in Supporting Information Figure S7.

To provide further support on self-aggregation of PMMA-*b*-Ptyr conjugate, we examined the DMF solution of the PMMA-*b*-Ptyr-I via DLS at different time intervals. The hydrodynamic diameter (D_h) of PMMA-*b*-Ptyr-I was found to be

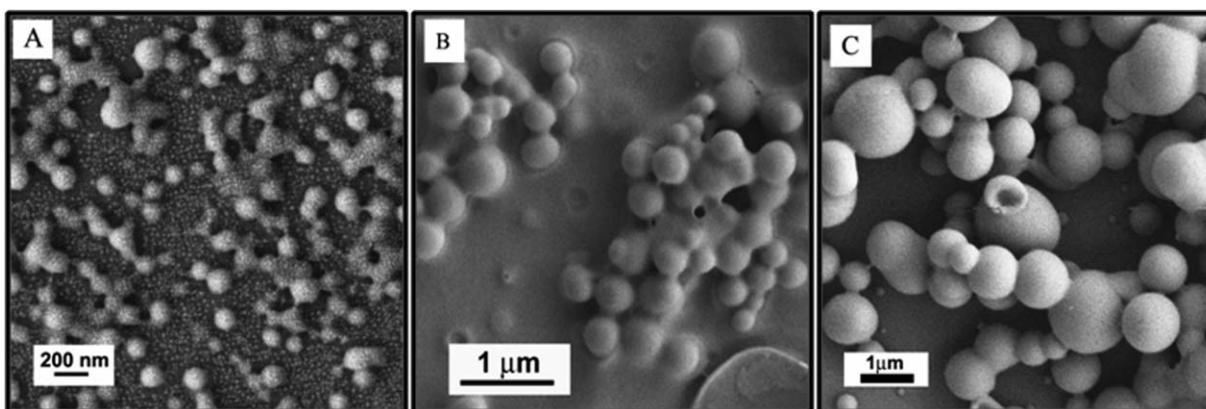
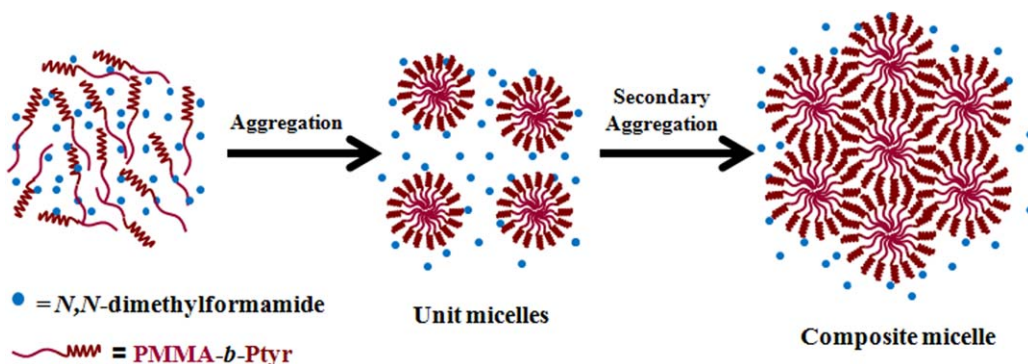


FIGURE 3 FESEM images of the self-aggregated PMMA-*b*-Ptyr-I conjugates in DMF (1 mg/mL) after keeping the solution undisturbed for different times (A) 30 min, (B) 4 h, and (C) 24 h.



SCHEME 2 Schematic representation for the formation of composite micelle in DMF. [Color figure can be viewed in the online issue, which is available at wileyonlinelibrary.com.]

331 nm after 30 min of aggregation (Supporting Information Fig. S8). But, the D_h s were unambiguously increased to 512 and 941 nm when we kept the conjugate MMF solution undisturbed for 4 and 24 h, respectively (Supporting Information Table S3 and Figure S8). Thus, DLS data showed a good correlation with that obtained from FESEM analysis.

Both the results of FESEM and DLS showed the increase of size of the formed micro/nanospheres upon increasing time of self-aggregation. Based on this observation and also from the literature survey including our earlier study,^{26,41} we can assume that the bigger spheres are nothing but composite or giant micelles, composed of initially formed unit micelles of PMMA-*b*-Ptyr block copolymer. The formation of such composite structure is owing to the further secondary interactions among unit micelles via H-bonding of amide groups between polypeptide chains as shown in Scheme 2. Unfortunately, we were unable to identify unit micelles experimentally, but we believe that the formation unit micelle is the first and necessary step for the generation of higher order composite micellar structure. Such unit micelle was formed because of the difference in polarity between PMMA and Ptyr chain with respect to DMF where Ptyr chain stretches toward the solvent front and PMMA chain remain inside the core of micelle (Scheme 2). We assume that the high interaction between the polytyrosine chains may be responsible for the formation of composite micelle at a faster rate by the combination of unit micelles. This is probably the reason for not observing any unit micelles experimentally.

Interestingly, the other two conjugates (PMMA-*b*-Ptyr-II and PMMA-*b*-Ptyr-III) containing shorter hydrophobic PMMA block were soluble in alkaline water (pH = 12.5) owing to the formation of phenolate ion. This provided us the opportunity to study the aggregation of these conjugates in water along with that study in DMF solution. The aggregated morphology of PMMA-*b*-Ptyr-II and PMMA-*b*-Ptyr-III conjugates in DMF was completely different to that of PMMA-*b*-Ptyr-I in DMF (Supporting Information Fig. S9). These results evidenced that the composition of PMMA and Ptyr block in the conjugate also affected the aggregation pattern in solution. As the Ptyr segment length is comparatively higher in the

cases of PMMA-*b*-Ptyr-II and PMMA-*b*-Ptyr-III conjugates, they assembled to a greater extent probably through hydrogen bonds between the OH groups of Ptyr block and the carbonyl groups of PMMA block that led to flake-like morphology. Similar types of interaction were also highlighted in the case of blend of Ptyr and poly(4-vinylpyridine), leading to the β -sheet type of secondary structures reported by Lu et al.³² Furthermore, at the optimum pH of \sim 12.5, PMMA-*b*-Ptyr-II and PMMA-*b*-Ptyr-III conjugates were soluble in water owing to the presence of tyrosinate ion in the Ptyr moiety, but remain strongly aggregated and exhibit indistinguishable aggregated morphology (Supporting Information Figs. S9A and S9B). The exact reason for the formation of such nanostructure may be owing to the formation of Na salt of Ptyr block. This results in strong ionic interaction among the Ptyr block of the conjugate as observed by Guo et al.⁴² in the case of poly(ethylene glycol)-*b*-poly(aspartic acid) conjugate.

Dye Encapsulation Study of Hybrid Micro/Nanospheres

To further investigate the mechanism of aggregation process, we studied the aggregation behavior in the presence of R6G dye. The fluorescence microscopic image of dye-encapsulated spherical composite micellar aggregates was compared with that of neat R6G dye solution (Supporting Information Fig. S10). It was very clear that there was a nice encapsulation of R6G molecules into the aggregated composite micelles during the time of aggregation of PMAA-*b*-Ptyr-I conjugate in DMF. From this study, we can further claim that the Ptyr blocks, which expose toward the solvent, eventually help the formation of composite micelles via secondary interaction and PMMA blocks reside in the core during aggregation (Scheme 2).

For further clarification on the encapsulation of R6G dye molecules into the aggregated micro/nanospheres, we also performed time-resolved fluorescence study of the R6G-loaded spheres and neat R6G in DMF using TCSPC. The time-resolved multiexponential fluorescence decay curves of neat R6G and R6G-encapsulated spheres were fitted according to the following equation and shown in Supporting Information Figure S11.

$$I(t) = \sum_{i=1}^N A_i \exp\left(\frac{-t}{\tau_i}\right)$$

where A_i and τ_i are the relative amplitude and lifetime of the i -th fluorescence component, respectively. N is the number of the fluorescence exponentials required for best nonlinear least squares fitting of the fluorescence decay curves. Average fluorescence lifetime (τ) was calculated from the decay times (τ_i) and the relative amplitudes (a_i) using the following relationship

$$\langle \tau \rangle = \tau_1 a_1 + \tau_2 a_2 + \tau_3 a_3$$

where τ_1 , τ_2 , and τ_3 are the component lifetimes and a_1 , a_2 , and a_3 are relative amplitudes, respectively.

Multieponential fluorescence decay curves showed the average life time of 3.7 ns for neat R6G, but an average life time of 3.978 ns in the case of R6G-encapsulated micro/nanospheres (Supporting Information Table S4). Increase in average life time for R6G-encapsulated spheres may arise owing to the interaction between dye molecules and conjugate molecules present in hybrid spheres. Such type of interaction may be ascribed from either H-bonding or dipole–dipole interaction between dye molecules and amide groups of P_{tyr} segment which stretch toward the periphery of micelles in solution.

CONCLUSIONS

We demonstrated the synthesis of PMMA-*b*-P_{tyr} copolymer conjugates of varying lengths of PMMA and P_{tyr} blocks via the combination of ATRP of MMA, “click” chemistry and ROP of tyrosine–NCA monomer. The GPC traces of azide end-functional PMMAs showed unimodal distribution with narrow polydispersities. The single peak in the GPC trace of PMMA-*b*-P_{tyr}-I conjugate confirmed that there was no any macroinitiator (PMAM-NH₂-1) remained after the completion of ROP of tyrosine–NCA. The relative compositions of MMA and Tyr units were determined from ¹H-NMR analysis. The self-aggregation of PMMA-*b*-P_{tyr} conjugate molecules in DMF resulted in the formation of micro/nanospheres as examined by FESEM and DLS study. The hybrid micro/nanospheres were actually the composite micelles formed by the aggregation of unit micelles of PMMA-*b*-P_{tyr} conjugate molecules owing to the difference in polarity of PMMA and P_{tyr} block, resulting in difference in solubility in DMF. The PMMA-*b*-P_{tyr} conjugates of longer P_{tyr} block lengths were soluble in alkaline water (pH = 12.5), which, upon standing, formed aggregated structures of indistinguishable morphology. The addition of an organic dye, R6G, during the aggregation of conjugates in DMF resulted in the formation of dye-encapsulated hybrid micro/nanospheres, which further ensured the aggregation of conjugate molecules. The dye encapsulation into micro/nanospheres was observed through fluorescence microscopy and average life-time measurement from TCSPC experiment. These polymer–polypeptide hybrid micro/nanospheres can be utilized in the field of delivery of dyes and drugs.

EXPERIMENTAL

Materials

MMA, α -bromoisobutyryl bromide, propargylamine, *N,N,N',N'',N'''*-pentamethyldiethylenetriamine (PMDETA), R6G, anhydrous copper(I) bromide (CuBr), and anhydrous copper(I) chloride were purchased from Sigma-Aldrich. 2-Chloro ethanol and sodium azide (NaN₃) were purchased from Merck, India. L-Tyrosine was received from SRL. All the chemicals were used as received unless otherwise mentioned. MMA was distilled under reduced pressure after washing with 5 wt % of aqueous NaOH prior to use. All the solvents were distilled and dried prior to use. All aqueous solutions were prepared with Milli-Q water.

Synthesis of Azide End-Functional PMMA (PMMA-N₃)

In a typical procedure, the molar ratio of the reactants is as follows: Monomer:Initiator:CuCl:PMDETA = 40:1:1:1. For PMMA-N₃ synthesis, typically, ABIB initiator (110.78 mg, 0.51 mmol) (for synthesis, see page S1 of Supporting Information ESI) and copper(I) chloride (50.56 mg, 0.51 mmol) were added to 3 mL of dry xylene in an oven-dried 25-mL long-necked round-bottomed flask. The reaction mixture was stirred and purged with N₂ gas for 30 min. PMDETA (106.6 μ L, 0.51 mmol) was then added to the round-bottomed flask and again purged with N₂ gas for 15 min until the solution became green in color. The mouth of the long-necked round-bottomed flask was carefully sealed with rubber septum after purging the reaction mixture and MMA (2.17 mL, 20.4 mmol) is injected via syringe through rubber septum. The reaction is schematically represented in Scheme 1. The whole reaction mixture was shifted to an oil-bath preheated to 90 °C and stirred for 48 h. After 48 h, the polymerization reaction was quenched by adding excess of THF and copper catalyst was carefully removed by passing the reaction mixture through basic alumina column using THF as the eluent. After being concentrated at rotary evaporator, the solution was precipitated into large amount of *n*-hexane and dried in vacuum oven at 50 °C for overnight to yield white product of PMMA-N₃ (yield = 1.988 g, 97%).⁴³ Finally, PMMA-N₃ of different molecular weights (Supporting Information Table S1) were successfully synthesized by the variation of ratio of [M₀]/[I₀] using same protocol.

Synthesis of Amino End-functional PMMA (PMMA-NH₂)

The PMMA-NH₂ was synthesized via copper-catalyzed azide-alkyne click reaction (CuAAC) with propargyl amine and PMMA-N₃ as shown in Scheme 1. In typical experiment, PMMA-N₃-I (300 mg, 0.05 mmol) and CuBr (21.52 mg, 0.15 mmol) were dissolved in 5 mL of dry THF with slow stirring in a two-necked round-bottomed flask whose mouth was attached with N₂ gas balloon. The solution was purged with N₂ gas for 15 min, PMDETA (32 μ L, 0.15 mmol) was then added to solution. The round-bottomed flask containing the reaction mixture was carefully degassed via three freeze-pump-thaw cycles to remove any traces of oxygen and was tightly sealed with a rubber septum. Propargyl amine (11.5 μ L, 0.18 mmol) was then injected into the solution by a syringe and stirred for 24 h at room temperature. The dark

green copper complex was removed by passing the reaction mixture through basic alumina column and the brown product was isolated by precipitation into hexane (yield = 75%).

Synthesis of PMMA-*b*-Ptyr Conjugate

Typically, tyrosine-NCA (0.16 g, 0.775 mmol) (Supporting Information ESI) was dissolved in 10 mL of dry DMF in two-neck round-bottomed flask. Sequentially, PMMA-NH₂-I (120.6 mg) was dissolved in 2 mL of dry DMF and was injected to the tyrosine-NCA solution at ice-bath via syringe. The reaction mixture was degassed via three freeze-pump-thaw cycles and stirred for 3 days at room temperature. At the end of complete reaction, the brown product was isolated by precipitation into diethyl ether and dried in vacuum oven at 35 °C (yield = 50%). Two other PMMA-*b*-Ptyr conjugates were also prepared by varying PMMA and Ptyr composition as summarized in Table 1. The synthesized and purified PMMA-*b*-Ptyr conjugates were characterized by NMR, FTIR, and GPC analyses.

ACKNOWLEDGMENTS

A. Saha sincerely thanks CSIR, India, for providing fellowship. This research is supported by grants from the CSIR, New Delhi, India. Thanks are also owing to the partial financial support from BRNS, India.

REFERENCES AND NOTES

- J. C. M. Van Hest, *Polym. Rev.* **2007**, *47*, 63–92.
- G. F. Chimonides, A. A. Sohdi, M. R. Khaleghi, C. R. Hurley, D. J. Adams, P. D. Topham, *J. Polym. Sci. Part A: Polym. Chem.* **2013**, *51*, 4853–4859.
- J. Y. Shu, B. Panganiban, T. Xu, *Annu. Rev. Phys. Chem.* **2013**, *64*, 631–657.
- J. D. Hartgerink, E. Beniash, S. I. Stupp, *Science* **2001**, *294*, 1684–1688.
- H. G. Börner, H. Schlaad, *Soft Matter* **2007**, *3*, 394–408.
- J.-F. Lutz, H. G. Börner, *Prog. Polym. Sci.* **2008**, *33*, 1–39.
- H.-A. Klok, *Macromolecules* **2009**, *42*, 7990–8000.
- H. Otsuka, Y. Nagasaki, K. Kataoka, *Curr. Opin. Colloid Interface Sci.* **2001**, *6*, 3–10.
- J. P. Jung, J. L. Jones, S. A. Cronier, J. H. Collier, *Biomaterials* **2008**, *29*, 2143–2151.
- A. V. Ambade, E. N. Savariar, S. Thayumanavan, *Mol. Pharm.* **2005**, *2*, 264–272.
- B. Apostolovic, S. P. E. Deacon, R. Duncan, H.-A. Klok, *Biomacromolecules* **2010**, *11*, 1187–1195.
- H. Dong, N. Dube, J. Y. Shu, J. W. Seo, L. M. Mahakian, K. W. Ferrara, T. Xu, *ACS Nano* **2012**, *6*, 5320–5329.
- S. Lecommandoux, M.-F. Achard, J. F. Langenwalter, H.-A. Klok, *Macromolecules* **2001**, *34*, 9100–9111.
- E.-K. Schillinger, E. Mena-Osteritz, J. Hentschel, H. G. Börner, P. Bäuerle, *Adv. Mater.* **2009**, *21*, 1562–1567.
- A. K. Shaytan, E.-K. Schillinger, P. G. Khalatur, E. Mena-Osteritz, J. Hentschel, H. G. Börner, P. Bäuerle, A. R. Khokhlov, *ACS Nano* **2011**, *5*, 6894–6909.
- K. Matyjaszewski, J. Xia, *Chem. Rev.* **2001**, *101*, 2921–2990.
- Y. Zhang, Y. Wang, C.-H. Peng, M. Zhong, W. Zhu, D. Konkolewicz, K. Matyjaszewski, *Macromolecules* **2012**, *45*, 78–86.
- S. Y. Kim, C. F. Zukoski, *Macromolecules* **2013**, *46*, 6634–6643.
- T. Smart, H. Lomas, M. Massignani, M. V. Flores-Merino, L. R. Perez, G. Battaglia, *Nano Today* **2008**, *3*, 38–46.
- H. Kühnle, H. G. Börner, *Angew. Chem. Int. Ed.* **2009**, *48*, 6431–6434.
- D. J. Siegwart, J. K. Oh, K. Matyjaszewski, *Prog. Polym. Sci.* **2012**, *37*, 18–37.
- C. Cummings, H. Murata, R. Koepsel, A. J. Russell, *Biomaterials* **2013**, *34*, 7437–7443.
- H. R. Kricheldorf, *Angew. Chem. Int. Ed.* **2006**, *45*, 5752–5784.
- T. J. Deming, *Adv. Mater.* **1997**, *9*, 299–311.
- D. J. Adams, D. Atkins, A. I. Cooper, S. Fuzeland, A. Trewin, I. Young, *Biomacromolecules* **2008**, *9*, 2997–3003.
- T. K. Paira, S. Banerjee, M. Raula, A. Kotal, S. Si, T. K. Mandal, *Macromolecules* **2010**, *43*, 4050–4061.
- R. Trzcinska, D. Szveda, S. Rangelov, P. Suder, J. Silberring, A. Dworak, B. Trzebicka, *J. Polym. Sci. Part A: Polym. Chem.* **2012**, *50*, 3104–3115.
- N. Hadjichristidis, H. Iatrou, M. Pitsikalis, G. Sakellariou, *Chem. Rev.* **2009**, *109*, 5528–5578.
- H.-A. Klok, J. F. Langenwalter, S. Lecommandoux, *Macromolecules* **2000**, *33*, 7819–7826.
- C.-J. Huang, F.-C. Chang, *Macromolecules* **2008**, *41*, 7041–7052.
- A. Nagai, D. Sato, J. Ishikawa, B. Ochiai, H. Kudo, T. Endo, *Macromolecules* **2004**, *37*, 2332–2334.
- Y.-S. Lu, Y.-C. Lin, S.-W. Kuo, *Macromolecules* **2012**, *45*, 6547–6556.
- G. Fuks, R. Mayap Talom, F. Gauffre, *Chem. Soc. Rev.* **2011**, *40*, 2475–2493.
- T.-B. Ren, W.-J. Xia, H.-Q. Dong, Y.-Y. Li, *Polymer* **2011**, *52*, 3580–3586.
- E. Amado, R. Schöps, W. Brandt, J. Kressler, *ACS Macro. Lett.* **2012**, *1*, 1016–1019.
- J. Hentschel, H. G. Börner, *J. Am. Chem. Soc.* **2006**, *128*, 14142–14149.
- T. K. Paira, S. Banerjee, T. K. Mandal, *J. Polym. Sci. Part A: Polym. Chem.* **2012**, *50*, 2130–2141.
- W. Agut, D. Taton, S. B. Lecommandoux, *Macromolecules* **2007**, *40*, 5653–5661.
- H.-A. Klok, H. Schlaad, Eds., In *Peptide Hybrid Polymers*; Springer: Berlin, Heidelberg, **2006**; pp 53–73.
- M. G. J. ten Cate, N. Severin, H. G. Börner, *Macromolecules* **2006**, *39*, 7831–7838.
- R. Erhardt, M. Zhang, A. Böker, H. Zettl, C. Abetz, P. Frederik, G. Krausch, V. Abetz, A. H. E. Müller, *J. Am. Chem. Soc.* **2003**, *125*, 3260–3267.
- X. Guo, L. Liu, W. Wang, J. Zhang, Y. Wang, S.-H. Yu, *CrystEngComm* **2011**, *13*, 2054–2061.
- M. Biswas, A. Saha, M. Dule, T. K. Mandal, *J. Phys. Chem. C* **2014**, *118*, 22156–22165.